Journal of Neurochemistry

JNC

JOURNAL OF NEUROCHEMISTRY | 2019 | 151 | 116–130

doi: 10.1111/jnc.14700

ORIGINAL ARTICLE

MicroRNA-135a-5p reduces $P2X_7$-dependent rise in intracellular calcium and protects against excitotoxicity

David Reigada*, Andrés Ángel Calderón-García*†, Manuel Soto-Catalán*, Manuel Nieto-Díaz*, Teresa Muñoz-Galdeano*, Ángela del Águila*‡ and Rodrigo M. Maza*

*Molecular Neuroprotection Group, Hospital Nacional de Parapléjicos, Servicio de Salud de Castilla La Mancha (SESCAM), Toledo, Spain

†Instituto de Neurociencias de Castilla y León (INCYL), Faculty of Medicine, University of Salamanca. Institute of Biomedical Research of Salamanca (IBSAL), Salamanca, Spain

‡Division of Developmental Biology, Cincinnati Children's Hospital Medical Center, Cincinnati, Ohio, USA

Abstract

Excitotoxic cell death because of the massive release of glutamate and ATP contributes to the secondary extension of cellular and tissue loss following traumatic spinal cord injury (SCI). Evidence from blockage experiments suggests that over-expression and activation of purinergic receptors, especially $P2X_7$, produces excitotoxicity in neurodegenerative diseases and trauma of the central nervous system. We hypothesize that the down-regulation of specific miRNAs after the SCI contributes to the over-expression of $P2X_7$ and that restorative strategies can be used to reduce the excitotoxic response. In the present study, we have employed bioinformatic analyses to identify microRNAs whose down-regulation following SCI can be responsible for $P2X_7$ over-expression and excitotoxic activity. Additional luciferase assays validated microRNA-135a-5p (miR-135a) as a posttranscriptional modulator of $P2X_7$. Moreover, gene expression analysis in spinal cord samples from a rat SCI model confirmed that the decrease in miR-135a expression correlated with $P2X_7$ over-expression after injury. Transfection of cultures of Neuro-2a neuronal cell line with a miR-135a inhibitory sequences (antagomiR-135a), simulating the reduction of miR-135a observed after SCI, resulted in the increase of $P2X_7$ expression and the subsequent ATP-dependent rise in intracellular calcium concentration. Conversely, a restorative strategy employing miR-135a mimicked reduced $P2X_7$ expression, attenuating the increase in intracellular calcium concentration that depends on this receptor and protecting cells from excitotoxic death. Therefore, we conclude that miR-135a is a potential therapeutic target for SCI and that restoration of its expression may reduce the deleterious effects of ATP-dependent excitotoxicity induced after a traumatic spinal cord injury.

Keywords: ATP, intracellular calcium, miRNA, neuroprotection, Purinergic receptors, spinal cord injury.

J. Neurochem. (2019) **151**, 116–130.

Injuries to the central nervous system (CNS) are the leading cause of permanent disability in developed countries (Ouzký 2002; DeVivo 2012). Cell death significantly contributes to neural damage and functional deficit in these pathologies (Grossman *et al.* 2001). Excitotoxicity is among the earliest processes leading to cell death after CNS trauma, triggered by the massive release of glutamate from neurons and glia, and the excessive and/or prolonged activation of NMDA receptors. This causes a lethal influx of calcium (Leonard and Salpeter, 1979; Orrenius *et al.*, 2003) resulting in the activation of necrotic, apoptotic, and autophagic death processes (Lipton and Rosenberg 1994; Prentice *et al.* 2015; Yildiz-Unal *et al.* 2015).

Received March 13, 2019; revised manuscript received March 15, 2019; accepted March 18, 2019.

Address correspondence and reprint requests to Dr Rodrigo M. Maza, Molecular NeuroprotectionGroup, Hospital Nacional de Parapléjicos, Servicio de Salud de Castilla La Mancha (SESCAM), Finca la Peraleda, s/n, 45071 Toledo, Spain. E-mail: rodrigom@sescam.jccm.es

Abbreviations used: $[Ca^{2+}]_i$, intracellular calcium concentration; 3′UTR, 3′ untranslated region; ATP, adenosine 5′-triphosphate; Bz-ATP, benzoylbenzoyl-ATP; DAPI, 4′,6-diamino-2-fenilindol; DPI, days post-injury; EGTA, ethylene glycol tetraacetic acid; HEPES, 4-(2-hydroxyethyl)-1-piperazineethanesulfonic acid; HRP, horseradish peroxidase; NMDA, N-methyl-D-aspartate; PBS, phosphate-buffered saline; RRID, research resource identifier (see scicrunch.org); RT-qPCR, real-time quantitative polymerase chain reaction; SCI, spinal cord injury; SDS-PAGE, sodium dodecyl sulfate-polyacrylamide gel electrophoresis; Sp1, specificity protein 1; WB, western blot.

Damage to the CNS also causes the release of large amounts of ATP and other nucleotides (Neary *et al.* 1996; Abbracchio and Burnstock 1998) that activate the purinergic receptors. As observed in NMDA receptors, overactivation of the purinergic receptors induces calcium influx and may lead to excitotoxic death in neurons (Zhang *et al.* 2005; Mitchell *et al.* 2009; Hu *et al.* 2010; Cisneros-Mejorado *et al.* 2015) and oligodendrocytes (Domercq *et al.* 2010) either directly or indirectly, favoring glutamate release (Cho *et al.*, 2010; Duan *et al.*, 2003; Gu and MacDermott, 1997).

Purinergic agonists, together with their specific membrane ionotropic (P2X) and metabotropic (P2Y) receptors, form a primitive system with a wide range of functions. Multiple purinergic receptors are expressed in the spinal cord (Apolloni *et al.*, 2009); some of which become over-expressed after injury (Cavaliere *et al.* 2003; Franke *et al.* 2006; Rodríguez-Zayas *et al.* 2010), including $P2X_7$ (Schwab *et al.* 2005; Gómez-Villafuertes *et al.* 2015). Blockage of $P2X_7$ and other purinergic receptors with either pyridoxalphosphate-6-azophenyl-2′,4′-disulfonic acid (PPADS), oxidized ATP (oxo-ATP), brilliant blue G (BBG), or the partial agonist Ap_4A provides neuroprotection in rat models of spinal cord injury (SCI) (Wang *et al.* 2004; Peng *et al.* 2009; Rodríguez-Zayas *et al.* 2011; Reigada *et al.* 2017) and traumatic brain injury (Wang *et al.* 2015). Results indicate that blockage reduces neuronal damage, microglial activation, neutrophil infiltration, and inflammatory response, leading to increased tissue preservation, although one study has failed to reproduce some of these effects (Marcillo *et al.* 2012).

RNA interference, a mechanism of post-transcriptional gene silencing, is an effective tool for protein inhibition, particularly for 'undruggable' proteins. Recent studies testing shRNAs or siRNAs silencing of $P2X_7$ resulted in improved outcomes in different types of CNS injuries (Feng *et al.* 2015; Liu *et al.* 2015; Zhao *et al.* 2016); microRNA (miRNA)-mediated silencing is an endogenous alternative to siRNA and shRNA. miRNAs are a family of small non-coding RNAs capable of silencing the expression of more than 60% of the protein-coding genes to regulate major cell processes, such as differentiation, proliferation, or death (Selbach *et al.* 2008; Sayed and Abdellatif 2011; Su *et al.* 2015). Many miRNAs are highly expressed in the mammalian CNS (Miska *et al.* 2004; Kosik 2006), where they play essential roles in virtually every function (Krichevsky 2007; Goldie and Cairns 2012). Changes in miRNA content are associated with alterations in the expression of their gene targets in a wide range of neurological diseases (Saugstad 2010; Meza-Sosa *et al.* 2012) and may contribute to deleterious events such as inflammation or apoptosis (Bhalala *et al.* 2013; Nieto-Diaz *et al.* 2014).

Therapies restoring miRNA expression have yielded promising results in animal models of CNS pathologies, successfully improving regeneration, protecting neural cells, and modulating astrogliosis after SCI (Bhalala *et al.* 2012; Jee *et al.* 2012a,b). Here, we hypothesize that (i) down-regulation of specific miRNAs after the SCI is at least partially responsible for the simultaneous over-expression of $P2X_7$ and other purinergic receptors, and therefore, that (ii) restoring the expression of $P2X_7$-silencing miRNAs reduces the excitotoxic response caused by the ATP-induced overactivation of the purinergic receptors. In fact, miRNAs silencing $P2X_7$ are potential therapeutic targets for various inflammatory, osteogenic, neuropsychiatric, pathogenic and neurodegenerative diseases (Volonté *et al.* 2012). To test the proposed hypotheses, we first combined predictive algorithms, computational tools, and expression data to establish which microRNAs undergo expression changes after SCI that may account for the over-expression of $P2X_7$ and the purinergic excitotoxicity. Results suggest that down-regulation of microRNA-135a-5p (miR-135a) may be a significant contributor to $P2X_7$ over-expression, and thus, identify this microRNA as a potential therapeutic target. To test this possibility, we employed antagomiRs to reduce miR-135a expression in Neuro-2a neuronal cell line cultures, simulating the changes observed after the SCI. Results confirm that miR-135a down-regulation causes $P2X_7$ over-expression and increases excitotoxicity when exposed to high concentrations of ATP. In contrast, over-expression of miR-135a using specific miRNA mimics leads to reduced $P2X_7$ and an amelioration of the calcium response to excitotoxic levels of ATP.

Material and methods

Bioinformatics and data mining

To predict microRNAs that can be therapeutic targets for reducing SCI excitotoxicity mediated by $P2X_7$, we combined computational tools with data mining of gene expression data. First, we carried out an *in silico* screening using four main prediction tools that employ existing databases and algorithms to predict miRNA candidates with sequence targets (MREs) in the 5′UTR and 3′UTR and the coding region of the mRNA of $P2X_7$. In this analysis, we employed miRanda (http://www.microrna.org), Target Scan (http://www.targetscan.org), miRDB (http://mirdb.org) and miRMap (http://mirmap.ezlab.org/) computer tools. Although different authors have cautioned against combining predictions (Alexiou *et al.* 2009; Witkos *et al.* 2011), they all acknowledge that such combinations result in enhanced specificity although at the price of reduced sensitivity (Alexiou *et al.* 2009).

miR-135a targeting on $P2X_7$ was further assessed by analyzing target site accessibility of the mRNA secondary structure (i.e., how likely a region in a mRNA sequence is accessible to miRNA binding). We employed mFold (Zuker 2003) to calculate the free energy of the binding site and to compare it with that of the 100 nucleotides flanking the 5′ and 3′ sides in the rat 3′UTR mRNA. We also studied target site accessibility using PITA software to estimate the Probability of Interaction by Target Accessibility (Kertesz *et al.* 2007). We also employed the miRmap program to calculate the minimal folding energy as a measurement of accessibility. miRmap predicts stable structures of miRNA–mRNA duplexes by computing

their minimum free energy (calculated with the Vienna RNA Secondary Structure Library (Lorenz *et al.* 2011).

Finally, we noted which microRNAs from the selected subset became down-regulated after SCI, matching the observed over-expression of $P2X_7$. In these studies, we employed published miRNA expression data from microarray analyses of a rat model of traumatic SCI. The data are available at the GEO database (http://www.ncbi.nlm.nih.gov/geo/), under accession number GSE19890. All data are MIAME-compliant. Detailed methods are published in Yunta and col (Yunta *et al.* 2012a).

Spinal cord injury model

In vivo procedures were performed in female Wistar rats (of 200 g of weight (12–14 weeks of age; RRID:RGD_13508588.). Animals were bred at the animal facility of the Research Unit and housed in plastic cages in a temperature and humidity controlled room maintained on a 12 : 12 h reverse light/dark cycle with free access to food and water. Animals were routinely authenticated by the animal facility service.

SCI surgery followed the methodology described in Yunta and col. (Yunta *et al.* 2012b). Briefly, following thoracic vertebra 8 (T8) laminectomy, rats were injured by a 200 KDyne contusion (IH Spinal Cord Impactor device from Precision System & Instrumentation, Lexington, KY, USA). After surgery, animals were maintained by daily manual bladder expression and by administration of the analgesic Buprenorphine (0.03 mg/Kg Buprex; Reckitt Benckiser Pharmaceuticals Limited, Richmond, VA, USA), and the antibiotic enrofloxazine (0.4 mg/Kg Baytril; Bayer AG, Leverkusen, Germany) up to 2 days after injury. Hind limb paralysis after injury was confirmed 2 days after the surgery using the Basso, Beattie, and Bresnahan 21-point locomotor score for rat models of spinal cord injury (Basso *et al.* 1995). We used a BBB value of 7 as the upper limit to include the animals in the gene expression analyses. Three experimental groups were agreed upon – 3 days post-injury (DPI), 7 DPI, and control – each comprising three individuals, enough to guarantee sufficient statistical power for real-time quantitative polymerase chain reaction (RT-qPCR) according to previous studies while avoiding unnecessary replication. After the experiment, we employed the obtained gene expression data to confirm this assumption, evaluating whether the agreed upon sample size was enough to reach a power level above 0.95 and a significance level below 0.05. Power calculations were performed a posteriori, that is, after conducting the experiments and gathering the data. To estimate statistical power, we employed the *post hoc* (a posteriori) analysis of G*Power 3.1 (Faul *et al.* 2007) to calculate Cohen's effect size f from the group size (3), the mean values for each group, and the average standard deviance. We employed the *F* test: Fixed effects ANOVA – one way routine of g-power software to calculate the Cohen's effect size index f from the data about group size, number of groups, mean value for each group, and average standard deviation. Parameters employed were number of groups = 3, sample size = 3/group, significance level = 0.05, estimated effect size=Cohen's f. Data on mean values and average standard deviation are detailed in Fig. 2b and c for each gene under analysis. Using these values, we estimated an effect size of $f = 1.85271$ and a power = 0.9696938 for the miR-135a expression data, and an effect size of $f = 4.167007$ and a power = 0.9977818 for $P2X_7$ expression data.

Animals were pseudorandomly distributed in the experimental groups following this procedure: each animal received an arbitrary number and was allocated to one of the experimental groups or a reserve group using a random sequence generated with www.random.org. The first three animals in the sequence were allocated to the control group, the second three to the 3 DPI group, the following three individuals formed the 7 DPI group, and the remaining individuals were ordered according to the random sequence to be employed as reserve individuals. The first reserve individual replaced one individual from the 7 DPI group that was excluded because of a suboptimal contusion reflected in an excessive locomotion recovery – above 7 in the BBB scale according to the settled exclusion criterion – in the tests performed 2 days after surgery.

Animals were subject to surgeries on different days so that all could be sampled on the same day (see the time line in Fig. 2a). All experimental procedures were in accordance with the European Communities Council Directive 2010/63/EU, Spanish Royal Decree 53/2013 (experimental animal use regulation) and Order ECC/566/2015 (regulation of personnel formation in animal experimentation) and were approved by the Hospital Nacional de Parapléjicos Animal Care and Use Committee (153BCEEA/2016).

Cell line and antibody sources

In this study, we employed the Neuro-2a (ATCC, Manassas, VA, USA, cat#:CCL-131; RRID:CVCL_0470) and HEK293T (ATCC, Manassas, VA, USA, cat#:CRL-1573; RRID:CVCL_0045) cell lines. Both cell types were experimentally used between passes 3 and 10. Neither Neuro-2a nor HEK293T cell lines are listed as commonly misidentified cell lines by the International Cell Line Authentication Committee (ICLAC; http://iclac.org/databases/cross-contaminations/) and were routinely authenticated through a STR profile analysis (ATCC).

We also used the following antibodies: anti-$P2X_7$ antibody (Alomone Labs, Jerusalem, Israel, cat#APR-008; RRID:AB_2040065), anti-β-tubulin antibody (Sigma-Aldrich, St. Louis, MO, USA, cat# T5293; RRID:AB_477580), horseradish peroxidase (HRP)-conjugated goat anti-rabbit antibody (ThermoFisher Scientific, Waltman, MA, USA, cat#31460; RRID:AB_228341), HRP-conjugated goat anti-mouse antibody (ThermoFisher Scientific, cat#31430; RRID:AB_228307), and Alexa Fluor 488 nm-conjugated goat anti-rabbit antibody (Molecular Probes, ThermoFisher Scientific, Cat# A11029; RRID:AB_10562715). We validated that anti-$P2X_7$ and anti-β-tubulin antibodies recognized the specific bands corresponding to their expected molecular weights (see Fig. S1).

Cell culture

All *in vitro* experiments were performed on the Neuro-2a cell line, a mouse neural crest-derived cell line commonly employed to study neuronal biology and signaling pathways (Tremblay *et al.* 2010). The one exception was for luciferase reporter assays for which we chose the human embryonic kidney HEK293T cell line because of its high rates of transfection. Both Neuro-2a and HEK293T cell lines were grown in Dulbecco's modified Eagle's medium (DMEM; Lonza, Basel, Switzerland) supplemented with 10% fetal bovine serum (FBS; Lonza) and 1% penicillin/streptomycin solution (Gibco, ThermoFisher Scientific, Waltham, MA, USA) at 37°C and 5% CO_2 according to ATCC recommendations.

Transfections and sample collection

The specific culture plates and cell densities and counts used in each experimental setting are described in their corresponding methodological section. Transfection was carried out according to the recommended procedures of Dharmafect-1 reagent (https://dharmacon.horizondiscovery.com/uploadedFiles/Resources/basic-dharmafect-protocol.pdf). In brief, cell cultures were transfected for 24 h with 50 nM of miRIDIAN microRNA rno-miR-135a-5p mimic (miR Base accession MIMAT0000841; Dharmacon cat#: C-320366-03-0005, mature sequence: 5′-uauggcuuuuuauuccuauguga) or antagomiR-135a inhibitory sequence (miRIDIAN rno-miR-135a-5p-Hairpin inhibitor; Dharmacon cat#:IH-320366-05-0002; mature sequence: 5′-uguagggauggaagccaugaaa) or a negative control sequence based in *C. elegans* cel-miR-67-3p with minimal sequence identity with any human, mouse, or rat miRNAs (miRIDIAN microRNA mimic negative control#1; miRBase accession#: MIMAT0000039; Dharmacon cat#:CN-001000-01-05; mature sequence: 5′-ucacaaccuccuagaaagaguaga) using DharmaFECT-1 reagent and associated protocols (Dharmacon, Lafayette, CO, USA).

RT-qPCR for miRNA and mRNA expression changes

To carry out RT-qPCR on spinal cord samples, three rats per experimental group (non-injured, 3 and 7 days post-injury) were sacrificed by sodium pentobarbital overdose. One cm long spinal cord fragments centered in the injury area were extracted. For the analyses of cell cultures, Neuro-2a cells were plated in 12 well plates. After reaching 80% confluence (3×10^5 cells/well), cultures were transfected for 24 h with a miR-135a mimic, an inhibitory sequence (antagomiR-135a), or a negative control sequences. Samples were coded by a member of the laboratory that did not participated in the RT-qPCR so that all subsequent processes were blinded for the researchers in charge of analyzing the samples.

Total RNA from samples of spinal cords and Neuro-2a cell cultures (10^6 cells per 35 mm dish) were extracted using the QiazolLysis Reagent (Qiagen) followed by purification using the miRNeasy Isolation Kit (Qiagen, cat#217004) according to manufacturer protocols (https://www.qiagen.com/us/resources/resourcedetail?id=d9c17dc7-6a0d-4728-9b04-9a6c9bc9e0e3&lang=en). RNA content in each sample was determined using an ND 1000 spectrophotometer (NanoDrop Technologies INC., Wilmington, DE, USA). For miRNA expression analysis, 10 ng of total extracted RNA was retrotranscribed to cDNA employing specific primers and the Taqman microRNA Reverse Transcription Kit (Fisher Scientific, cat#10524815) (1 × RT-PCR cycle: 30 min at 16°C plus 30 min at 42°C plus 5 min at 85°C) following the company protocols (https://www.thermofisher.com/order/catalog/product/4366596). To measure P2X$_7$ gene expression, 1 ug of total RNA was treated with DNase I (Roche; Bassel, Switzerland) for 30 min at 37°C plus 3 min at 95°C and then retrotranscribed by incubation with Moloney leukemia virus transcriptase (Invitrogen, Carlsbad, CA, USA) and Primer Random mix (Roche, cat# 11034731001) for 60 min at 37°C plus 3 min at 95°C. The amplification reaction was performed following the ΔΔCt routine (see details in: https://assets.thermofisher.com/TFS-Assets/LSG/manuals/4364016.pdf) in a TaqMan 7900HT Fast Real-Time PCR System (Applied Biosystems, Foster City, CA, USA) using the TaqMan Universal PCR Master Mix, no AmpErase UNG (Fisher Scientific, cat#4324018) together with commercial specific FAM-MBG conjugated probes (Life Technologies, Carlsband, CA, USA; rat P2X7 probe for spinal cord expression (cat#4331182, Rn00570451_m1) or mouse probe for expression in Neuro-2a cell line (cat#4331182, Mm01199500_m1)). The reactions were programmed in the 9600 emulation mode, that is, first 10 min at 95°C, followed by 40 cycles of a two-step amplification run, comprising 15 s at 95°C, plus 1 min at 60°C.

Both miRNA and mRNA data were analyzed following the methods from Livak and Schmittgen (Livak and Schmittgen 2001). Briefly, we determined the difference (ΔCt) between the cycle threshold of the target mRNA or miRNA and their respective endogenous loading controls – U6 small nuclear RNA for miRNAs and 18S ribosomal RNA for mRNA – and its associated variance following the standard propagation of error method from Headrick and col. (Headrick 2010). Then, we compared the ΔCt value from different times post-injury with the ΔCt from non-injured animals (0 DPI) to calculate the ΔΔCt and the correspondent fold increase ($2^{-\Delta\Delta Ct}$), indicating also the 95% confidence interval. Statistical analysis was performed using a one-way ANOVA with Tukey *post hoc* test.

Luciferase/renilla assay for validation of miRNAs regulation on P2X$_7$ expression

The 3′UTR sequence of the P2X$_7$ mRNA (3′UTR-P2X$_7$) was amplified by PCR from total rat brain DNA extract using the forward *gccacattatggtgactc* and reverse *ggtggtagtggtagtg* primers and subcloned in the pmiR-Glo vector (Dual-Luciferase microRNA Target Expression Vector, Promega, Madison, WI, USA). All the employed constructions will be shared upon reasonable request. Constructions were grown in *E.coli DH5*cells and isolated using the EndoFree Plasmid Maxi Kit (Qiagen, cat#12362). 50 nM of miRNA mimic or a negative control (C-) were co-transfected with 2 μg/mL of p-miR^{P2X7} (pmiR-Glo vector with the 3′UTR-P2X$_7$ inserted) or p-miR^0 (empty pmiR-Glo vector) in HEK293T cells at 80% confluence (5×10^4 cells per well in 96-well plate) using the DharmaFECT Duo Transfection Reagent (Dharmacon). After 24 h, the firefly luciferase and renilla luciferase light emission ratio (Dual Luciferase Reporter Assay System, Promega) was measured using a spectrophotometer plate reader (Infinite M200, Tecan Group LTD. Mannedorf, Switzerland). Firefly luciferase/renilla luciferase ratios were normalized vs. double negative control condition (pmir-Glo^0 + C-).

Western blot

Neuro-2a cell cultures at 80% confluence (3×10^5 cells per well in 12-well plate) were transfected for 24 h with either miR-135a mimic, antagomiR-135a, or the negative control. Total protein was extracted using mechanical detachment of the cells followed by lysis with a RIPA (radioimmunoprecipitation assay buffer, Sigma-Aldrich, St. Louis, MO, USA) containing a protease inhibitor cocktail (Complete cocktail, Roche). The obtained homogenates were cleared by centrifugation (10 000 *g* for 15 min at 4°C) and the protein content was determined by the bicinchoninic acid method (Pierce BCA Protein Assay Kit, ThermoFisher Scientific, cat#23227). As described for RT-qPCR analyses, following extraction, the samples were coded by a member of the laboratory not involved in the western blot (WB) analyses to guarantee the blinding of that all subsequent processes.

Cell homogenates containing 50–100 μg of protein were separated using conventional sodium dodecyl sulfate-polyacrylamide gel electrophoresis (10% acrylamide/bisacrylamide and 10% sodium dodecyl sulfate), in reducing conditions (5% β-mercaptoethanol; Sigma-Aldrich) and transferred to polyvinylidenedifluoride membranes (Immobilon, Merk Millipore; Darmstadt, Germany). Membranes were blocked in blocking buffer (5% non-fat milk diluted in phosphate-buffered saline (PBS)-T buffer (0.05% Tween-20 (Sigma-Aldrich) in PBS)). Target proteins were detected by overnight incubation at 4°C with a solution of anti-$P2X_7$ (1 : 500) or anti-β-tubulin antibodies (loading control, 1 : 1000) diluted in blocking buffer. Afterward, membranes were washed twice in PBS-T buffer and incubated at RT for 1 h with a solution of HRP-conjugated goat anti-rabbit (1 : 10 000) or HRP-conjugated goat anti-mouse antibodies (1 : 10 000) diluted in blocking buffer. After two washes in PBS-T, HRP signal was developed using an enhanced chemiluminescence detection system (ECL; Pierce, ThermoFisher Scientific) and images were acquired with the Image Scanner III and the LabScan v6.0 software (GE Healthcare Bio-Sciences, Chicago, IL, USA). Band densities were determined using the ImageJ 1.51n software (National Institutes of Health, NIH; (Schneider *et al.* 2012) and normalized versus the β-tubulin values for each sample.

Immunofluorescence

Neuro-2a cells were cultured over 12 mm round coverslips inside a 24-well plate. After reaching 80% confluence (3×10^4 cells per coverslip), cultures were transfected for 24 h with miR-135a mimic, antagomiR-135a, or the negative control sequence. Then, cells were fixed with 4% paraformaldehyde for 20 min at RT and then permeabilized and blocked by incubation overnight at 4°C with blocking buffer (5% goat serum (Sigma-Aldrich) and 0.2% Triton X-100 (Sigma-Aldrich) in PBS). The cell were then incubated for 2 h at RT in a solution of anti-$P2X_7$ antibody (1 : 500) diluted in blocking buffer, followed by three washes in PBS and an incubation in a solution of secondary antibody Alexa Fluor 488 nm-conjugated goat anti-rabbit (1 : 500), diluted in blocking buffer. Finally, coverslips were mounted on glass slides employing Fluorescence Mounting Medium (DAKO North America Inc. Aligent Technologies Inc., Carpinteria, CA, USA) with 1:3000 of the fluorescent marker of nucleic acids 4′,6-diamino-2-fenilindol (Sigma-Aldrich). Preparations were imaged in an epifluorescence microscope (DM5000B, Leica Microsystem GmbH, Wetzlar, Germany) with a ×40 objective and analyzed using ImageJ 1.51n software. To estimate protein expression in individual cells, we employed phase contrast images to place a 3 μm diameter circular ROI on the cytoplasm of the chosen cells and then measured the intensity of Alexa 488 emission in the corresponding image. We measured a total of 300 and 40 cells per condition in antagomiR and mimic experiments, respectively (numbers are indicated in the text).

Measurement of intracellular calcium concentration

Neuro-2a cells were cultured in 96-well plates. After reaching 80% confluence (5×10^4 cells per well), cultures were transfected with either a miR-135a mimic, an antagomiR-135a, or a negative control sequence. After 24 h, cells were incubated with 10 μM Fura 2-AM (ThermoFisher Scientific, cat# F-1221) and 0.2% pluronic acid in Krebs' solution pH = 7.4 for 30 min at 37°C (Sigma-Aldrich, cat#2443). Krebs' solution was composed of 105 mM NaCl (Sigma-Aldrich), 5 mM KCl (Sigma-Aldrich), 10 mM Na-HEPES (Merk), 5 mM $NaHCO_3$ (Sigma-Aldrich), 60 mM mannitol (Sigma-Aldrich), 5 mM sucrose (Sigma-Aldrich), 0.5 mM $MgCl_2$ (Sigma-Aldrich), and 1.3 mM $CaCl_2$ (Sigma-Aldrich). After two washes with Krebs' solution, rise in $[Ca^{2+}]_i$ was induced with ATP or the $P2X_7$-specific agonist benzoylbenzoyl-ATP (Bz-ATP; Sigma-Aldrich), added to each well through the internal injector system of the spectrophotometer plate reader (Infinite M200, Tecan Group LTD. Mannedorf, Switzerland). $[Ca^{2+}]_i$ was estimated by alternatively exciting cells at 340 and 380 nm and measuring the fluorescence emission at 510 nm at 37°C in the plate reader. Calcium concentrations at the baseline and the peak were calculated from the 340/380 ratio (R), first subtracting autofluorescence baseline emission in the absence of Fura 2-AM and then employing the formula developed by Grynkiewicz and col. (Grynkiewicz *et al.* 1985) and following the formula:

$$[\mathrm{Ca2+]i(nM)} = \mathrm{Kd} \times \left(\frac{R_x - R_{\min}}{R_{\max} - R_x}\right) x \left(\frac{380_{\min}}{380_{\max}}\right)$$

where K_d(of Fura 2-AM)corresponds to 350×10^{-9} M (Negulescu and Machen 1990); R_x is the ratio for each well and time; R_{min} corresponds to the ratio obtained by bathing cells in 'minimum buffer' (Krebs' buffer containing 10 mM EGTA (Sigma-Aldrich) and 5 μM ionomycin (Sigma-Aldrich), pH = 8.0); R_{max} corresponds to the ratio calculated after bathing the cells in 'maximum buffer' (Krebs' buffer containing 5 μM ionomycin, pH = 8.0); and 380_{min} and 380_{max} correspond to the 510 nm emission values measured after 380 nm excitation in cells bathed with 'minimum buffer' and 'maximum buffer', respectively. Calibration was performed separately for each plate. Increase in $[Ca^{2+}]_i$ after agonist addition (peak) was expressed as a ratio relative to the pre-addition baseline concentration (increase=peak-baseline/baseline). To assess the effects of antagomiR or mimic, we compared the response to ATP or Bz-ATP in cells transfected with a negative control with the response in cells transfected with antagomiR or mimic oligonucleotides. In each experiment, the increase measured in the treatment cells was expressed as a ratio relative to the response of the control cells. Statistical analyses were carried out comparing the response values in treated (mimic or antagomiR) and control cells for each experiment following a paired design. No blinding procedure was introduced in these experiments.

Cell death assays

Neuro-2a cells were grown in 48-well plates. After reaching 80% confluence (10^6 cells per well), cultures were transfected with a miR-135a mimic or a negative control sequence. Twenty-four hours after transfection, cell death was induced by incubation with 300 μM Bz-ATP for 3 h. After mechanical detachment, we followed manufacturer instructions to stain cells with Annexin V DY634 kit (Immunostep, Salamanca, Spain, cat#ANXVDK-100T) to detect the translocation of membrane phosphatidylserine occurring in early apoptotic stages and with SYTOX Blue Dead Cell Stain (ThermoFisher Scientific, cat#S34862) a marker of compromised membranes associated to late apoptotic stages. The extent of the cell death processes, estimated from the number of Annexin V and/or SYTOX positive cells, was analyzed by flow cytometry. A dot plot

(a)

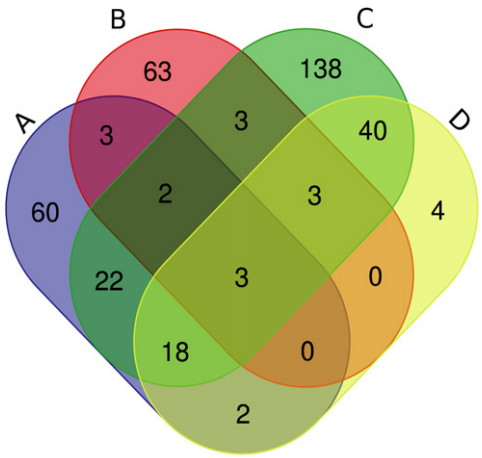

(b)

	B. miRDB	C. miRanda	D. miRMap	A. TargetScan	
	Percentile	Score	Score (perc.)	Score (perc.)	Aggr. PTC
miR-135a-5p (nt.940)	73	–0.22	–0.06 (65.70)	–0.14 (57)	<0.1
miR-124-3p (nt.1047)	74	–0.497	–0.21 (96.56)	–0.35 (89)	<0.1
mir-24-3p (nt. 189)	90	–0.102	–0.23 (97.38)	–0.21 (73)	<0.1

miR-135a-5p (nt.940)			
mFold	mean ΔG	100 bp 5′	100 bp 3′
	–12.97	–22.5	–26.3
PITA	ΔG Duplex	ΔG Open	ΔΔG
	–15.5	–9.2	–6.3
D. miRMap	ΔG binding	ΔG Open	ΔG total
	–12.98	18.59	6.39

(c)

rno miR135a-5p 3′ aguguauc**CUUAUUUUUCGGUA**u 5′

rno 3′UTR P2X$_7$ nt: 935 5′ auuaacca**GACU - AGAAGCCAU**c

mmu 3′UTR P2X$_7$ nt: 935 5′ auuaacca**GACU - AGAAGCCAU**c

hsa 3′UTR P2X$_7$ nt: 307 5′ ua**GCAGGG**CUGC**AGUAGCCAU**g 3′

Fig. 1 Predicted miRNA candidates with MREs in the 3′UTR-P2X7. (a) Venn diagram showing the number of miRNAs with MREs in the 3′UTR-P2X7 predicted by different algorithms. Only three candidates were predicted by all four algorithms (miR-124-3p, miR-135a-5p, and miR-24-3p). (Algorithms used: TargetScan (a); miRDB (b); miRMap (c); and miRanda (d)). (b) localization of the different MREs for miR-135a in the whole sequence of the rat 3′UTR-P2X7, indicating the ΔΔG score for miRNA-target interactions, computed as the free energy gained by transitioning from the state in which the miRNA and the target are unbound (ΔGopen) and the state in which the miRNA binds its target (ΔGduplex). In (c), we represent the miR-135a sequence and its most accessible MRE located in nucleotide 935 in the rat 3′UTR-P2X7, also showing a high level of conservation between species (mouse (nt. 935) and human (nt. 307). The nucleotides are indicated in bold with complementarity for miR-135a.

showing pulse width versus area was used to distinguish between single cells and aggregates. A total of 10 000 gated single events were collected using a FACS Canto II flow cytometry (BD Biosciences, Franklin Lakes, NJ, USA) and the FACS Diva 6.1 software (BD Biosciences) and analyzed with Flow Jo Software (Celeza GmbH, Olten, Switzerland) to determine the percentage of population stained with each dye.

Data analysis

All data are expressed as mean ± SEM or mean ± SD as indicated in figure legends. Statistical significance of the treatment effects was tested using paired or non-paired Student's *t*-test or an analysis of variance test (ANOVA) depending on the characteristics of the data. Normality and homoscedasticity of the data were assessed using Shapiro–Wilk and Bartlett or *F* tests, respectively, using the Shapiro.test, Bartlett.test, var.test functions of R. Mann–Whitney–Wilcoxon test was employed to substitute Student's *t*-test when data were deemed non-parametric (immunofluorescence data following miR-135 over-expression). We employed Grubbs' test (also known as extreme Studentized deviate test method, available online at https://www.graphpad.com/quickcalcs/grubbs1/) to search for outliers among the analyses data. Statistical analyses and graphics were carried out using Prism Software 5 (GraphPad Software Inc., La Jolla, CA, USA) and R statistical language (*R* Core Team 2014). Differences were considered statistically significant when the p-value < 0.05.

Results

miR-135a is a candidate to regulate P2X$_7$ expression after SCI

In 2015, Miras-Portugal group described an increase in P2X$_7$ receptor expression after SCI which likely contributes to extending excitotoxicity during secondary injury (Gómez-Villafuertes *et al.* 2015; Miras-Portugal *et al.* 2016). Using *in silico* strategies, we searched for miRNAs with response elements (MREs) in the mRNA sequence of rat P2X$_7$, including the 3′UTR and 5′UTR regions and the coding region. Analysis with four different algorithms (In Fig. 1a,

TargetScan (a); miRDB (b); miRMap (c); and miRanda (d)) resulted in more than 500 candidates with predicted MREs in the 3′UTR-P2X$_7$ (no one in 5′UTR or coding region). Among them, miR-124-3p, miR-135a-5p, and miR-24-3p were predicted by all four algorithms.

Next, we employed our microarray data from a previously published study (Yunta *et al.* 2012b) to examine the expression of these three miRNAs in a rat model of spinal cord injury. According to these analyses, both miR-124-3p and miR-135a-5p, but not miR-24-3p, become down-regulated after the trauma in correlation with the P2X$_7$ over-expression observed by the Miras-Portugal group (Gómez-Villafuertes *et al.* 2015; Miras-Portugal *et al.* 2016). Therefore, we decided to discard miR-24-3p from additional analyses in this study. Moreover, we decided to focus all subsequent analyses on miR-135a-5p, reserving miR-124-3p for future study.

Analyses of target site accessibility of the mRNA secondary structure further supported miR-135a-5p (miR-135a) targeting on P2X$_7$. PITA algorithms suggested that miR-135a have several potential MREs with favorable ΔΔGs, particularly a site starting in the nucleotide 940 of the 3′UTR-P2X$_7$. Specific analyses for nucleotide 940 MRE confirm its accessibility (Fig. 1b), taking into account that the energy required to open the target mRNA secondary structure is smaller than the energy gained by the miRNA binding ($\Delta G_{open} = -9.2$ kcal/mol vs. $\Delta G_{duplex} = -15.5$ kcal/mol) leading to a net gain of energy ($\Delta\Delta G = -6.3$ kcal/mol). mFold results agreed with this prediction, taking into account that the free energy of the binding miR-135a-P2X$_7$ (mean $\Delta G = -13$ kcal/mol) in nucleotide 940 is clearly higher than in the 100 nucleotides flanking the 5′ and 3′ sides of the predicted miRNA binding site ($\Delta G = -22.5$ and -26.3 kcal/mol, respectively, Fig. 1b), also evidencing the accessibility of this MRE. Moreover, the minimal folding energy estimated by miRmap also predicted a stable structure for the miR-135a–P2X$_7$ duplex ($\Delta G_{total} = 6.39$ kcal/mol). Therefore, all employed algorithms suggest that microRNA-135a had several different predicted MREs with highly favorable ΔΔG values (Fig. 1b), particularly the one in nucleotide 935 of the 3′UTR-P2X$_7$, which in addition is highly conserved in different mammalian species, including rats, mice, and humans (Fig. 1c).

Decreased miR-135a expression after SCI correlated with P2X$_7$ over-expression

Expression data obtained after RT-qPCR analyses of RNA samples from control (0 DPI) and 3 and 7 days post-injury (3 and 7 DPI) spinal cords confirmed Miras-Portugal group results, showing a post-injury increase in P2X$_7$ expression that was statistically significant at 7 DPI (Fig. 2b). Parallel analysis of miR-135a expression showed a significant decrease at both 3 and 7 DPI, in agreement with our previous microarray data (Fig. 2c). Adjustment of a linear model to the RT-qPCR data revealed that miR-135a expression has a significant effect on the expression of P2X$_7$, in addition to the effect at the time after injury (Fig. 2d).

miR-135a targets 3′UTR-P2X$_7$ sequence

We next validated the effective binding of miR-135a to the 3′UTR-P2X$_7$ and its effect on the receptor expression. To carry out this analysis, we first inserted a construct including the firefly luciferase gene under the regulation of the promoter 3′UTR-P2X$_7$. Then, HEK293T cells were simultaneously co-transfected with (i) pmiR-Glo plasmid with (pmiR^{P2X7}) or without (pmiR^0) 3′UTR-P2X$_7$-Luciferase construct and (ii) miR-135a or negative control (C-) mimics.

Data shown in Fig. 3 demonstrate that co-transfection of a miR135a mimetic with pmiR^{P2X7} plasmid induced a significant 10.18 ± 4.71% reduction of luciferase activity relative to C- mimic and pmiR^{P2X7} co-transfection (Ratio luciferase/renilla: pmiR^{P2X7}+miR135a mimic = 105.00 ± 10.76; Ratio luciferase/renilla pmiR^{P2X7}+ C- mimic = 116.8 ± 11.85; $t_6 = 2.32$, $p = 0.0029$ in paired *t*-test (pmiR^{P2X7}+ C- vs. pmiR^{P2X7}+miR135a), $n = 3$ independent experiments with two replicates each). No effect from endogenous miRNAs (without mimic co-transfection) was detected on the luciferase activity of pmiR-Glo plasmids, with or without 3′UTR-P2X$_7$ insert (pmiR^{P2X7} and pmiR^0 plasmids, respectively). Moreover, transfection with miR-135a or C- mimics did not change the intrinsic luciferase activity of pmiR-Glo plasmids without P2X$_7$ insert (pmiR^0+ C- and pmiR^0+miR-135a).

Reduction of miR-135a expression induces P2X$_7$ over-expression

Previous analyses validate that miR-135a targets P2X$_7$; therefore, it may reduce the expression of this purinergic receptor and the ATP-dependent excitotoxic process induced by SCI, as hypothesized. To confirm the functional effect of the decrease of miR-135a detected in SCI on P2X$_7$ expression levels, we employed an *in vitro* approach using the mouse neuroblastoma cell line Neuro-2a that was, among different rat and mouse cell lines tested, the one that better fulfilled the requirements of a low expression of miR-135a and significant levels of P2X$_7$ receptor (data not shown). The use of a mouse neuronal cell line was supported by the fact that miR-135a MREs targets were conserved between the rat and mouse 3′UTR-P2X$_7$ (Fig. 1c).

To emulate the decrease in miR-135a induced by SCI, we transfected Neuro-2a cells with antagomiR-135a, a chemically modified oligonucleotide that binds to miR-135a and ensures its degradation. Following antagomiR administration, RT-qPCR data showed a significant 2.87-fold decrease in miR-135a expression together with a nearly significant 2.89-fold increase in P2X$_7$ receptor expression (Fig. 4a). Effects on P2X$_7$ receptor expression was confirmed at protein levels by both WB and immunofluorescence assays. WB data showed a significant increase of 63.17 ± 17.42% after antagomiR-135a transfection (t2 = 4.704; $p = 0.0212$

(a)

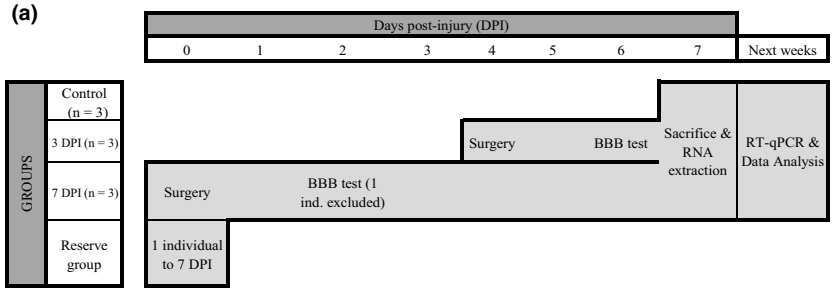

(b)

	ΔCt	One-Way ANOVA	Tukey's post-test	Mean diff (ΔΔCt)	*p*-value	fold change	
0 DPI	12.69 ± 0.13	$F_{2,6}$ = 48.93	3 DPI versus 0 DPI	–0.44 (–0.91,0.03)	$p > 0.05$ (n.s.)	1.36	(0.98,1.88)
3 DPI	12.25 ± 0.02	p = 0.0002	7 DPI versus 0 DPI	–1.49 (–1.97,–1.02)	$p < 0.001$ (***)	2.81	(2.03,3.92)
7 DPI	11.20 ± 0.30	***	7 DPI versus 3 DPI	–1.05 (–1.53,–0.57)	$p < 0.01$ (**)	2.07	(1.48,2.88)

(c)

	ΔCt	One-Way ANOVA	Tukey's post-test	Mean diff (ΔΔCt)	*p*-value	fold change	
0 DPI	7.01 ± 0.97	$F_{2,6}$ = 14.77	3 DPI versus 0 DPI	2.8 (1.21,4.39)	$p < 0.01$ (**)	0.14	(0.05, 0.43)
3 DPI	9.81 ± 0.40	p = 0.0048	7 DPI versus 0 DPI	1.64 (0.05,3.23)	$p < 0.05$ (*)	0.32	(0.11, 0.97)
7 DPI	8.65 ± 0.49	**	7 DPI versus 3 DPI	–1.16 (–2.75,0.43)	$p > 0.05$ (n.s.)	2.23	(0.74, 6.72)

(d)

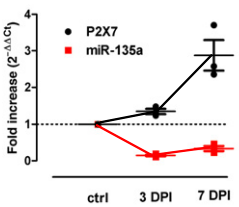

	Df	Adj. R Sq	*F* value	*p*-value
	3 and 5	0.867	18.34	0.004

	Df	Sum Sq	Mean Sq	*F* value	Pr(>*F*)
miR-135a	1	0.43	0.43	6.63	0.049
DPI	1	3.1	3.1	48.28	0.0009
miR-135a:DPI	1	0.007	0.007	0.11	0.75
Residuals	5	0.32	0.06		

Fig. 2 Over-expression of P2X$_7$ is related to decreased miR-135a expression in a rat model of contusive SCI. Each line in the graphical time line (a) corresponds to the time course of each experimental group and the reserve group, detailing the times of surgery procedures, behavioral tests, sample acquisition, RT-qPCR, and data analysis. One member from the 7 DPI group was replaced with a reserved individual that was excluded because of a suboptimal contusion reflected in an excessive locomotion recovery – above 7 in the BBB scale according to a settled exclusion criterion – in the tests performed 2 days after surgery. The replacement individual underwent all programmed procedures and tests at the same times and under the same conditions as the members of the 7 DPI group becoming *de facto* a member of this group. Tables showing the gene expression data of P2X$_7$ (b) and miR-135a (c) obtained after RT-qPCR analysis of spinal cords sampled at different DPIs (n = 3 animals per group with 3 technical replicates each). Tables also depict the results of statistical analysis of the effect of DPI on gene expression employing an ANOVA test. *post hoc* power analyses for one-way ANOVA test in G*Power software indicated that the analysis of P2X$_7$ (a) has a power of 0.991 (Effect size f = 2.095) whereas analysis of miR-135a has a power of 0.977 (f = 1.914). (d) dot plot graph shows the relationship between changes in expression levels (ΔC_t) of miR-135a (relativized to the housekeeping U6 snRNA) and P2X$_7$ (relativized to the housekeeping 18S rRNA) at 3 and 7 DPI (data were normalized against non-injured rat samples). Each point corresponds to one individual and lines the mean±SEM. Both genes were measured simultaneously in each sample. The attached table shows the linear model adjusted to the relationship of P2X$_7$ expression with miR-135a expression at the different DPIs. Results of the analysis revealed a significant model ($p < 0.01$; adjusted R^2 = 0.867; n = 3 animals per group with 3 technical replicates each), with both miR-135a expression and DPI significantly contributing to determine P2X$_7$ expression.

in a paired t-test; n = 3 independent experiments) (Figs 4b and c). Analysis of immunofluorescence images showed a significant 19.37% increase in P2X$_7$ staining intensity (t_{28} = 6.59, $p < 0.001$, n = 13–17 images per condition and 10 cells per image) in cells transfected with antagomiR-135a (100.1 ± 0.96 arbitrary units of fluorescence (A.U.F.)) relative to C- transfected cells (83.85 ± 0.83 A.U.F.) (Fig. 4d and e).

To determine the functional effect of the increase of P2X$_7$ receptor expression by antagomiR-135a transfection, we evaluated the changes in $[Ca^{2+}]_I$ induced by the activation of purinergic receptors as a response to excitotoxic levels of ATP (Fig. 4f and g). Fura 2-AM fluorescent determinations of $[Ca^{2+}]_i$ indicated that 300 μM ATP induced a 188.25 ± 31.74% rise in $[Ca^{2+}]_i$ relative to baseline levels in Neuro-2a cells transfected with negative

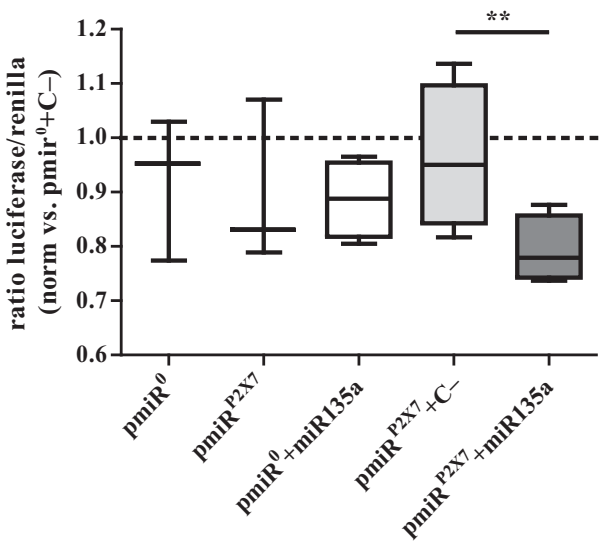

Fig. 3 Validation of the effective binding of miR-135a to its MREs in the 3′UTR-P2X$_7$. Luciferase reporter assay after co-transfection of HEK293T with (i) empty p-miR-Glo (pmiR^0) or pmiR-Glo + 3′UTR-P2X$_7$ (pmiR^{P2X7}) and (ii) miR-135a mimic or negative control (C-) mimics. Firefly and renilla activities were measured using the Dual-Luciferase Reporter Assay System (Promega), and finally, the firefly/renilla ratios were normalized versus double negative control condition (pmiR^0+ C-; dotted line). Data show a significant reduction in luciferase ratio following treatment with miR-135a mimic (pmiR^{P2X7}+miR-135a; dark gray filled bar) in comparison with C- transfection (pmiR^{P2X7}+ C-; light gray filled bar). Data from control conditions revealed that endogenous miRNAs have no effects on pmiR-Glo vector activity with (pmiR^{P2X7}) or without (pmiR^0) 3′UTR-P2X$_7$ insert, and that mimic co-transfection does not change the intrinsic luciferase activity of pmiR-Glo vector (pmiR^0+ C- and pmiR^0+miR-135a). (**$p < 0.01$ in paired *t*-test; $n = 3$ independent cell culture preparations).In the box plots, the upper and lower boundaries of the box represent the upper and lower quartile of the data, respectively, whereas the line within the box marks the median, and the whiskers above and below the box represent the maximum and minimum values, respectively.

control mimic. Transfection with antagomiR-135a induced a 57.01 ± 0.25% significant increase of the ATP effect (a 294.36 ± 48.58% rise from baseline levels; t9 = 2.0524; $p = 0.035$ in a paired *t*-test; $n = 10$ independent experiments). ATP is the most effective agonist of almost all purinergic receptors present in the cell, including P2X and P2Y receptors. In order to discriminate the effect of antagomiR-135a transfection specifically on P2X$_7$ receptor expression, we used the more P2X$_7$-specific agonist Bz-ATP (Fig. 4h and i). 100 μM Bz-ATP induced a 31.79 ± 0.14% significant increase of the Bz-ATP effect in antagomiR-135a transfected Neuro-2a cells (240.74 ± 0.14% from baseline levels) compared to negative control transfected cells (195.17 ± 37.44% from baseline levels; t9 = 2.429; $p = 0.019$ in a paired *t*-test; $n = 10$ independent experiments).

Increased levels of miR-135a reduce P2X$_7$ expression and function

Results from antagomiR-135a experiments confirm that decreasing miR-135a expression results on P2X$_7$ over-expression, a mechanism that may contribute to P2X$_7$-mediated excitotoxicity after SCI. Can we expect the opposite? That is, can we expect that a therapy restoring the basal levels of miR-135a will ameliorate the adverse effects of P2X$_7$ over-expression after SCI. To test this hypothesis, we evaluated the effects of administering a miR-135a mimic on the expression of P2X$_7$ and the excitotoxicity mediated by this purinergic receptor in cultures of Neuro-2a cells.

Transfection of miR-135a mimic in Neuro-2a cells is not able to induce any decrease in P2X$_7$ receptor expression at mRNA level (1.22-fold decrease compared levels in C- transfected cells; Fig. 5a), but significantly reduces its expression at protein levels as revealed by WB (54.25 ± 9.60% vs. C- transfected cells; t_2=3.4, $p = 0.038$, paired *t*-test, $n = 3$ independent experiments, Fig. 5b and c). Analysis of immunofluorescence images confirmed the reduction in P2X$_7$ protein expression, showing a significant reduction (32.43%; W = 1125, $p = 0.0002$, Mann–Whitney–Wilcoxon test or Wilcoxon rank-sum test, n = 15–20 images per condition and 5–10 cells per image); Fig. 5d and e) in P2X$_7$ staining intensity in cells transfected with miR-135a mimic (29.17 ± 2.42 A.U.F.) compared to C- transfected cells (43.17 ± 3.04 A.U.F.).

To determine the functional effects of reducing P2X$_7$ expression through miR-135a mimic transfection, we first evaluated the changes $[Ca^{2+}]_i$ induced by the activation of purinergic receptors like P2X$_7$. In order to measure the effects mediated by the specific changes in P2X$_7$ receptor expression, we stimulated the cultures with Bz-ATP. Determination of $[Ca^{2+}]_i$ in Neuro-2a cells transfected with the negative control mimic (C-) indicated that 100 μM Bz-ATP induced an 896.79 ± 255.38% rise in $[Ca^{2+}]_i$ from basal levels. Transfection with miR-135a mimic reduced this increase in $[Ca^{2+}]_i$ to 301.68 ± 91.49%, that is, miR-135a caused a significant 60.19 ± 6.78% reduction of the Bz-ATP effect (t_3=5.3, $p = 0.0066$, paired *t*-test; $n = 5$ independent experiments; Fig. 5f and g).

To explore the neuroprotective effects of this reduction, we tested whether miR-135a mimic transfection reduced Bz-ATP-induced excitotoxic death in Neuro-2a cells. According to our analyses, treatment of control (C- transfected) cells with 300 mM Bz-ATP for 3 h caused a threefold increase in the number of Annexin V positive cells and a twofold increase in SYTOX positive cells (Fig. 6a and b) reflecting the activation of apoptotic and/or necrotic death processes by Bz-ATP. Transfection of the cells with miR-135a mimic markedly reduced the number of Annexin V

(a)

		ΔCt	*T*-test (Tukey's post-test)			Fold decreasee
				mean diff (ΔΔCt)	*p* -value	
miR-135a	C–	11.92 ± 0.61	C–versus antagomiR	–1.52 (–3.20 , 0.16)	t_3 = 2.89 p = 0.032 (*)	2.87 (0.89,9.2)
	antagomiR-135a	13.44 ± 0.51				
P2X$_7$	C–	8.95 ± 1.28	C–versus antagomiR	–1.53 (–3.95 , 0.89)	t_4 = 1.753 p = 0.077 (n.s.)	2.89 (0.53,15.45)
	antagomiR-135a	7.57 ± 1.59				

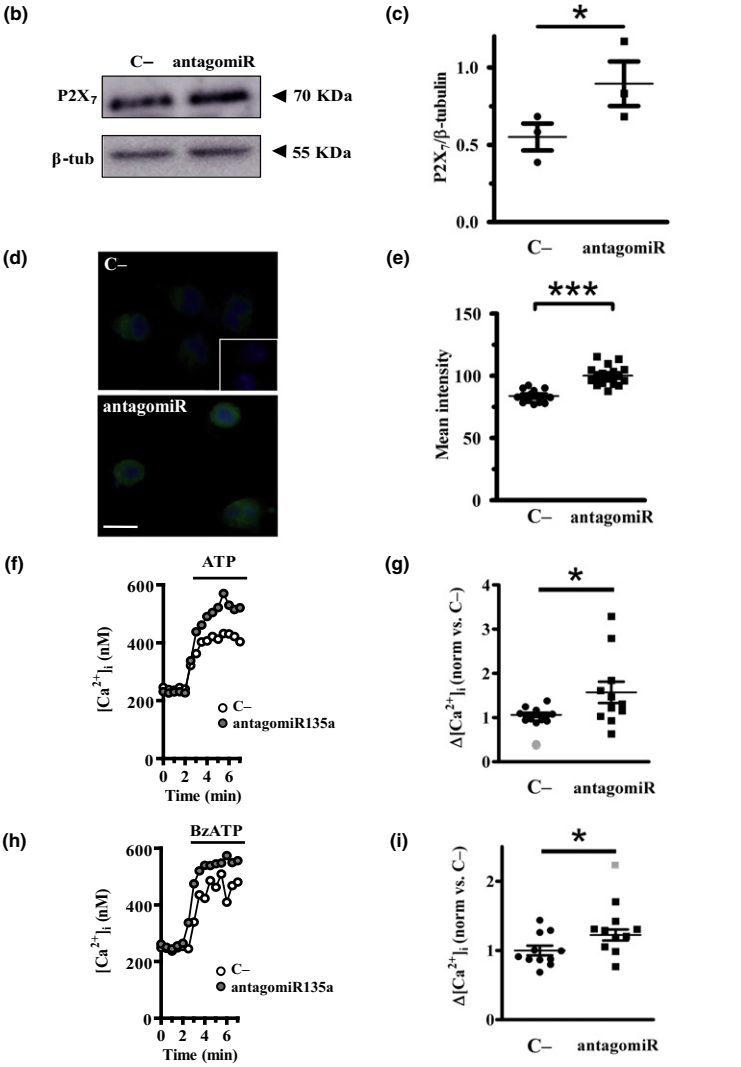

Fig. 4 Effect of miR-135a inhibition on P2X$_7$ expression and function in Neuro-2a cell line. (a) RT-qPCR results revealing the changes in P2X$_7$ and miR-135a gene expression of Neuro-2a cells cultures after transfection with antagomiR-135a. The table also depicts the results of the statistical analysis of these changes employing a *t*-test. Representative western blot (b) and dot plot summary (with mean±SEM represented) (c) of expression levels of P2X$_7$ in protein samples extracted from Neuro-2a cells 24 h after transfection. Densitometry band measurements were normalized by β-tubulin levels for each sample; *$p < 0.05$ (paired *t*-test; $n = 3$ independent cell culture preparations). These effects are also observed by immunofluorescence assays of P2X$_7$ expression in Neuro-2a cells, as shown in representative images (d). The associated dot plot graph (e) illustrates the significant increase in P2X$_7$ protein levels observed after antagomiR-135a transfection (squares) compared with negative control mimic transfected cells (C-; circles). Lines correspond to mean ± SEM; ***$p < 0.001$ (*t*-test; $n = 12$–16 fields of three independent cell culture preparations per condition (about 300 cells per condition)). Insert in (d) shows control of secondary antibody signal without anti-P2X$_7$ primary antibody. Bar scale = 10 μm. Representative traces of changes in $[Ca^{2+}]_i$ ($\Delta[Ca^{2+}]_i$) induced by ATP (f) and Bz-ATP (h) in Neuro-2a cells after 24 h of transfection with antagomiR-135a (gray filled circles) or negative control mimic (C-;empty circles). Dot plot summary (with mean±SEM represented) data reveal that miR-135a inhibition (circles) led to a decrease of the $\Delta[Ca^{2+}]_i$ induced by ATP (g) and Bz-ATP (i), in comparison with C- transfected cells (squares) ($n = 10$ independent cell culture preparations). Gray circles and squares in G and I represent the outlier data and that have been subtracted from the statistical calculations.

(a)

	ΔCt	Tukey's post-test			Fold change ($2^{-\Delta\Delta Ct}$)
			mean diff (ΔΔCt)	*p* value	
C-	7.29 ± 0.27	C–versus miR-135a	–0.29 (–1.64,1.06)	t_4=0.59 *p*=0.29 (n.s.)	1.22 (0.47,3.11)
miR-135a	7.01 ± 0.54				

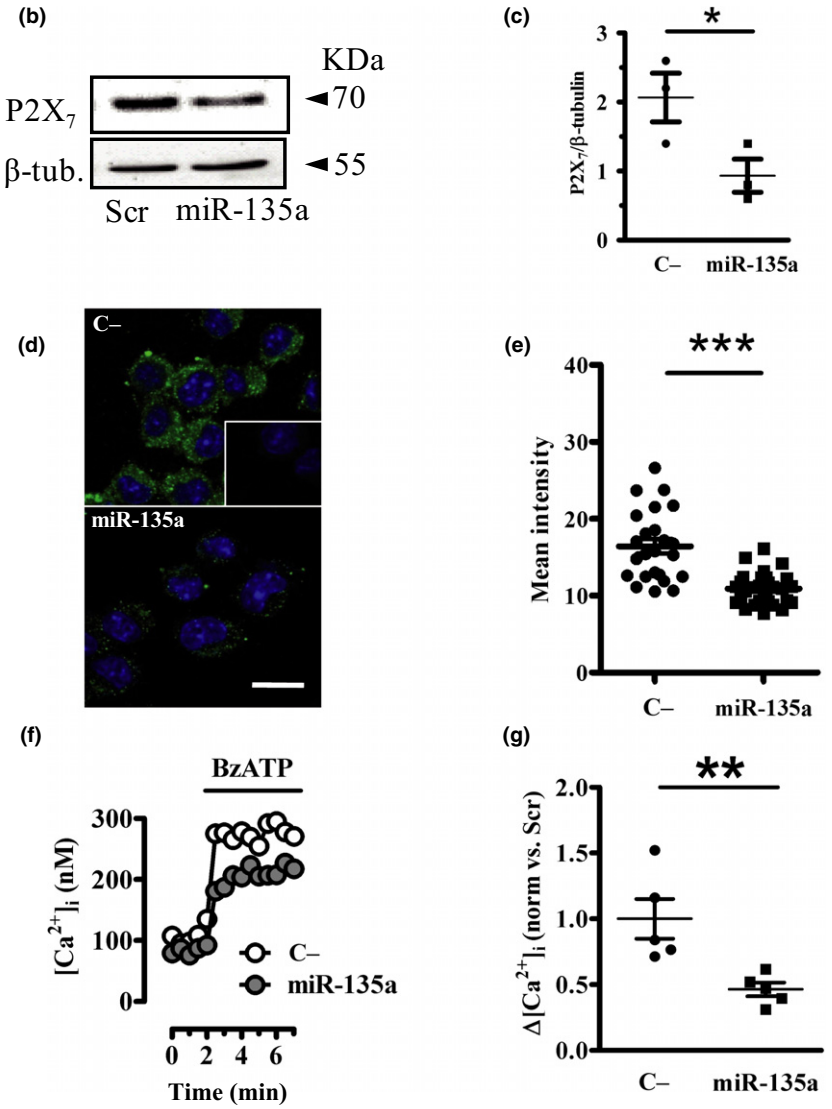

Fig. 5 Effect of miR-135a over-expression on $P2X_7$ expression and function in Neuro-2a cell line. (a) RT-qPCR results revealing the changes in $P2X_7$ gene expression of Neuro-2a cells cultures after transfection with miR-135a mimic. The table also depicts the results of the statistical analysis of these changes employing a *t*-test. Representative western blot (b) and dot plot summary (with mean±SEM represented) (c) of expression levels of $P2X_7$ in protein samples extracted from Neuro-2a cells 24 h after transfection. Densitometry band measurements were normalized by β-tubulin levels for each sample; $*p < 0.05$ (paired *t*-test; $n = 3$ independent cell culture preparations). These effects are also observed by immunofluorescence assays of $P2X_7$ expression in Neuro-2a cells, as shown in representative images (d). Insert shows control of the secondary antibody signal without anti-$P2X_7$ primary antibody. Bar scale = 10 μm. The associated dot plot graph (e) illustrates the significant increase in $P2X_7$ protein levels observed after miR-135a mimic transfection (squares) compared with negative control mimic transfected cells (C-; circles). Lines correspond to mean ± SEM; $***p < 0.001$ (*t*-test; $n = 9$–12 fields of three independent cell culture preparations per condition (about 40 cells per condition)). Representative traces of changes in $[Ca^{2+}]_i$ ($\Delta[Ca^{2+}]_i$) induced by Bz-ATP (f) in Neuro-2a cells after 24 h of transfection with miR-135a mimic (gray filled circles) or negative control mimic (C-;empty circles). Dot plot summary (with mean±SEM represented) reveals that miR-135a mimic transfection (squares) led to a decrease of the $\Delta[Ca^{2+}]_i$ induced by Bz-ATP (g), in comparison with C- transfected cells (circles). ($n = 3$ independent cell culture preparations with 3 replicates each)

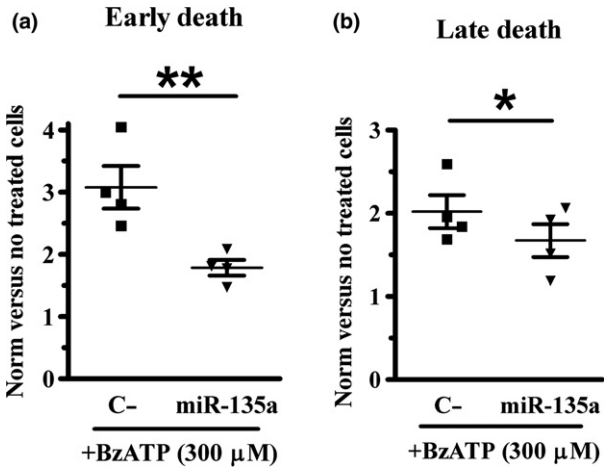

Fig. 6 Effect of miR-135a-induced decrease of P2X$_7$ expression on cell death in Neuro-2a cell line. Excitotoxic effect of the rise in $[Ca^{2+}]_i$ induced by Bz-ATP was evaluated by flow cytometry. Dot plot summary of results show that miR-135a mimic transfection (squares) induced a decrease in both early (Annexin V) (a) and late (SYTOX) (b) stages of apoptotic death induced by Bz-ATP (300 μM), in comparison with transfection of negative control mimic (C-; circles). Each point corresponds to the replicate mean of one independent experiment and lines the mean±SEM. *$p < 0.05$; **$p < 0.01$ in paired *t*-test; $n = 4$ independent cell culture preparations with two replicates each.

positive cells (t_3=5.62, $p = 0.006$, $n = 4$ independent experiments with two replicates each; paired *t*-test), and, to a minor extent, the number of SYTOX positive cells (t_7=2.42, $p = 0.047$, paired *t*-test; $n = 4$ independent experiments with two replicates each), confirming the cytoprotective effects of increasing miR-135a expression.

Discussion

A previous analysis from our laboratory and others (Liu *et al.* 2009; Strickland *et al.* 2011; Yunta *et al.* 2012b) revealed that SCI leads to the dysregulation of numerous miRNAs, several involved in modulating cell fate (Bhalala *et al.* 2013; Bhalala 2015). The present work aimed to determine whether miRNA dysregulation contributes to P2X$_7$-mediated excitotoxicity and whether restoring miRNA levels can reduce the expression and activity of this purinergic receptor. The bioinformatic analyses carried out in the present study suggest that one of the miRNAs down-regulated after SCI, miR-135a, may target P2X$_7$. P2X$_7$ is a microRNA expressed in a wide range of mammal species, including human, rat or mouse, and has been previously validated as regulator of proteins implicated in inflammation (Feng *et al.* 2015), ischemia (Zhu *et al.* 2015), hypoxia (Gonsalves and Kalra 2010), or apoptosis (Zhao *et al.* 2014; Chu *et al.* 2015; Liu *et al.* 2017) as well as in Alzheimer's (Liu *et al.* 2014) and Parkinson's diseases (Liu *et al.* 2016). Luciferase reporter assays confirmed the presence of miR-135a response elements in the 3′UTR of the mRNA of P2X$_7$. Interestingly, the target sequences in P2X$_7$ mRNA identified in rodents are conserved across different mammalian species, including humans, so that any therapeutic tool developed for animal models may also function in humans. Our bioinformatics analyses also indicated that miR-124, another miRNA strongly down-regulated after SCI (Nakanishi *et al.* 2010; Yunta *et al.* 2012b), likely targets the 3′UTR-P2X$_7$ sequence, although we still have to validate the predicted MRE sequences.

RT-qPCR of RNA samples from rat spinal cords obtained after traumatic SCI confirmed the reduction of miR-135a expression already described (Yunta *et al.* 2012b) and the increase of P2X$_7$ expression described by the Miras-Portugal laboratory (Gómez-Villafuertes *et al.* 2015; Miras-Portugal *et al.* 2016). Results also suggest that both changes are inversely correlated, although such correlation is far from complete, indicating that miR-135a down-regulation is not the only miRNA or mechanism responsible for the P2X$_7$ expression changes taking place after SCI (see, for example, Zhou *et al.* 2009).

To confirm the direct impact of miR-135a down-regulation on P2X$_7$ expression, we complemented the RT-qPCR and reporter assays with loss-of-function analyses in the neuronal cell line Neuro-2a. In agreement with observations in the damaged spinal cord, administration of antagomiR-135a – a synthetic oligonucleotide complementary to the mature target miR-135a that silences its expression (Krützfeldt *et al.* 2005; Mattes *et al.* 2007) – led to an increase of P2X$_7$ protein expression in Neuro-2a cultures.

All these results support the first hypothesis of this study, that is, that down-regulation of specific miRNAs after the SCI is at least partially responsible for the over-expression of P2X$_7$ and suggest that restoration of miR-135a levels may reduce P2X$_7$ over-expression and its mediated excitotoxicity. In recent years, many restorative therapies have been developed aiming to replace depleted miRNAs with synthetic miRNA mimics under the assumption they can assume the regulatory roles of natural miRNAs in the repression of target protein expression (Peng *et al.* 2015), with promising results in oncology (Beg *et al.* 2017). Therefore, we devoted the second part of this study to testing the hypothesis that a restorative therapy designed to recover the expression levels of miR-135a lost after SCI would reduce the deleterious effects of the Ca2+-dependent excitotoxic processes induced by the activation of the over-expressed P2X$_7$ receptor.

Gain-of-function analyses employing miRNA mimic technology to over-express miR-135a in cultures of Neuro-2a cells led to a reduction of P2X$_7$ expression and the P2X$_7$-dependent rise in $[Ca^{2+}]$i. Moreover, it also reduced both early and late stages of P2X$_7$-induced apoptotic death. Altogether, these results confirm that restoring miR-135a expression after traumatic SCI may reduce ATP-induced P2X$_7$-mediated excitotoxicity and

protect neural cells. There are multiple selective antagonists for the $P2X_7$ receptor that may result in improved blockage (see review in (North and Jarvis 2013). miR-135a-based therapies may complement these drugs and reduce the risk of resistance in due course. Restoring the pre-injury levels of miRNAs also has the advantage that the mimics employed in these therapies have the same sequence as the dysregulated miRNAs. As such non-specific off-target effects are not expected. Moreover, because every miRNA inhibits the expression of hundreds of mRNAs to regulate cell state, miRNA restorative therapies extend far beyond the 'one target, one drug' paradigm, with additional positive effects expected. However, multiple aspects still remain to be elucidated. On the one hand, administration of miR-135a mimics significantly reduces $P2X_7$ expression at protein levels but does not seem to affect transcript abundance. This observation is not surprising, as it is well known that miRNA-mediated gene silencing can occur through mRNA degradation, translation repression, or an interplay of both (Jonas and Izaurralde 2015). However, it leaves the genetic over-expression of $P2X_7$ observed after SCI unexplained. As previously mentioned, there are many other mechanisms that can be acting to increase the gene expression of this receptor, including the inhibition of other miRNAs such as miR-124 as well as the activation of transcriptional regulators such as Sp1 factor (see Miras-Portugal *et al.*, 2016 for review and hypotheses). Additional *in vivo* research is needed to establish the implication of these alternative miRNAs and/or mechanisms as well as to validate the actual effects of miRNA modulation in the damaged spinal cord.

Acknowledgments and conflict of interest disclosure

This work was supported by: Instituto de Salud Carlos III, through the project PI12/02828 and a grant from the Fundación Tatiana Pérez de Guzmán el Bueno. We thank for their technical and logistic support to the Fundación del Hospital Nacional de Parapléjicos para la Investigación y la Integración (FUHNPAIIN) and the microscopy, flow cytometry, and animal facilities of the Experimental Neurology Unit, Hospital Nacional de Parapléjicos, Toledo, Spain. The authors declare that they have no conflicts of interest with the contents of this study.

All experiments were conducted in compliance with the ARRIVE guidelines.

Supporting information

Additional supporting information may be found online in the Supporting Information section at the end of the article.

Figure S1. Changes in miR-135a expression induced changes in the expression of P2X7receptor.

References

Abbracchio M. P. and Burnstock G. (1998) Purinergic signalling: pathophysiological roles. *Jpn. J. Pharmacol.* **78**, 113–145.

Alexiou P., Maragkakis M., Papadopoulos G. L., Reczko M. and Hatzigeorgiou A. G. (2009) Lost in translation: an assessment and perspective for computational microRNA target identification. *Bioinformatics* **25**, 3049–3055.

Apolloni S., Montilli C., Finocchi P. and Amadio S. (2009) Membrane compartments and purinergic signalling: P2X receptors in neurodegenerative and neuroinflammatory events. *FEBS J.* **276**, 354–364.

Basso D. M., Beattie M. S. and Bresnahan J. C. (1995) A sensitive and reliable locomotor rating scale for open field testing in rats. *J. Neurotrauma* **12**, 1–21.

Beg M. S., Brenner A. J., Sachdev J., Borad M., Kang Y.-K., Stoudemire J., Smith S., Bader A. G., Kim S. and Hong D. S. (2017) Phase I study of MRX34, a liposomal miR-34a mimic, administered twice weekly in patients with advanced solid tumors. *Invest. New Drugs* **35**, 180–188.

Bhalala O. G. (2015) Chapter 26: The emerging impact of microRNAs in neurotrauma pathophysiology and therapy, in *Brain Neurotrauma Mol. Neuropsychol. Rehabil. Asp.*, (Kobeissy F., ed), pp. 349–367. CRC Press, Taylor & Francis, Boca Raton, FL.

Bhalala O. G., Pan L., Sahni V., McGuire T. L., Gruner K., Tourtellotte W. G. and Kessler J. A. (2012) microRNA-21 regulates astrocytic response following spinal cord injury. *J. Neurosci.* **32**, 17935–17947.

Bhalala O. G., Srikanth M. and Kessler J. A. (2013) The emerging roles of microRNAs in CNS injuries. *Nat. Rev. Neurol.* **9**, 328–339.

Cavaliere F., Florenzano F., Amadio S. *et al.* (2003) Up-regulation of P2X2, P2X4 receptor and ischemic cell death: prevention by P2 antagonists. *Neuroscience* **120**, 85–98.

Cho J.-H., Choi I.-S. and Jang I.-S. (2010) P2X7 receptors enhance glutamate release in hippocampal hilar neurons. *Neuroreport* **21**, 865–870.

Chu Y.-Y., Ko C.-Y., Wang W.-J., Wang S.-M., Gean P.-W., Kuo Y.-M. and Wang J.-M. (2015) Astrocytic CCAAT/enhancer binding protein δ regulates neuronal viability and spatial learning ability via miR-135a. *Mol. Neurobiol.* **53**, 4173–4188.

Cisneros-Mejorado A., Pérez-Samartín A., Gottlieb M. and Matute C. (2015) ATP signaling in brain: release, excitotoxicity and potential therapeutic targets. *Cell. Mol. Neurobiol.* **35**, 1–6.

Core Team R. (2014) *R: A Language and Environment for Statistical Computing*. Austria, Vienna.

DeVivo M. J. (2012) Epidemiology of traumatic spinal cord injury: trends and future implications. *Spinal Cord* **50**, 365–372.

Domercq M., Perez-Samartin A., Aparicio D., Alberdi E., Pampliega O. and Matute C. (2010) P2X7 receptors mediate ischemic damage to oligodendrocytes. *Glia* **58**, 730–740.

Duan S., Anderson C. M., Keung E. C., Chen Y., Chen Y. and Swanson R. A. (2003) P2X7 receptor-mediated release of excitatory amino acids from astrocytes. *J. Neurosci.* **23**, 1320–1328.

Faul F., Erdfelder E., Lang A.-G. and Buchner A. (2007) G*Power 3: a flexible statistical power analysis program for the social, behavioral, and biomedical sciences. *Behav. Res. Methods* **39**, 175–191.

Feng L., Chen Y., Ding R., Fu Z., Yang S., Deng X. and Zeng J. (2015) P2X7R blockade prevents NLRP3 inflammasome activation and brain injury in a rat model of intracerebral hemorrhage: involvement of peroxynitrite. *J. Neuroinflammation* **12**, 190.

Franke H., Krügel U. and Illes P. (2006) P2 receptors and neuronal injury. *Pflugers Arch.* **452**, 622–644.

Goldie B. J. and Cairns M. J. (2012) Post-transcriptional trafficking and regulation of neuronal gene expression. *Mol. Neurobiol.* **45**, 99–108.

Gómez-Villafuertes R., Rodríguez-Jiménez F. J., Alastrue-Agudo A., Stojkovic M., Miras-Portugal M. T. and Moreno-Manzano V. (2015) Purinergic receptors in spinal cord-derived ependymal stem/progenitor cells and their potential role in cell-based therapy for spinal cord injury. *Cell Transplant.* **24**, 1493–1509.

Gonsalves C. S. and Kalra V. K. (2010) Hypoxia-mediated expression of 5-lipoxygenase-activating protein involves HIF-1alpha and NF-kappaB and microRNAs 135a and 199a-5p. *J. Immunol.* **184**, 3878–3888.

Grossman S. D., Rosenberg L. J. and Wrathall J. R. (2001) Temporal-spatial pattern of acute neuronal and glial loss after spinal cord contusion. *Exp. Neurol.* **168**, 273–282.

Grynkiewicz G., Poenie M. and Tsien R. Y. (1985) A new generation of Ca2 + indicators with greatly improved fluorescence properties. *J. Biol. Chem.* **260**, 3440–3450.

Gu J. G. and MacDermott A. B. (1997) Activation of ATP P2X receptors elicits glutamate release from sensory neuron synapses. *Nature* **389**, 749–753.

Headrick T. C. (2010) Statistical simulation: power method polynomials and other transformations, in *Journal of Statistical Software* (Demirtas H., ed), pp. 1–174. Chapman & Hall/CRC, Boca Raton, FL.

Hu H., Lu W., Zhang M. *et al.* (2010) Stimulation of the P2X7 receptor kills rat retinal ganglion cells in vivo. *Exp. Eye Res.* **91**, 425–432.

Jee M. K., Jung J. S., Choi J. I., Jang J. A., Kang K. S., Im Y. and Bin Kang S. K. (2012a) MicroRNA 486 is a potentially novel target for the treatment of spinal cord injury. *Brain* **135**, 1237–1252.

Jee M. K., Jung J. S., Im Y., Bin Jung S. J. and Kang S. K. (2012b) Silencing of miR20a is crucial for Ngn1-mediated neuroprotection in injured spinal cord. *Hum. Gene Ther.* **23**, 508–520.

Jonas S. and Izaurralde E. (2015) Towards a molecular understanding of microRNA-mediated gene silencing. *Nat. Rev. Genet.* **16**, 421–433.

Kertesz M., Iovino N., Unnerstall U., Gaul U. and Segal E. (2007) The role of site accessibility in microRNA target recognition. *Nat. Genet.* **39**, 1278–1284.

Kosik K. S. (2006) The neuronal microRNA system. *Nat. Rev. Neurosci.* **7**, 911–920.

Krichevsky A. M. (2007) MicroRNA profiling: from dark matter to white matter, or identifying new players in neurobiology. *Sci. World J.* **7**, 155–166.

Krützfeldt J., Rajewsky N., Braich R., Rajeev K. G., Tuschl T., Manoharan M. and Stoffel M. (2005) Silencing of microRNAs in vivo with 'antagomirs'. *Nature* **438**, 685–689.

Leonard J. P. and Salpeter M. M. (1979) Agonist-induced myopathy at the neuromuscular junction is mediated by calcium. *J. Cell Biol.* **82**, 811–819.

Lipton S. A. and Rosenberg P. A. (1994) Excitatory amino acids as a final common pathway for neurologic disorders. *N. Engl. J. Med.* **330**, 613–622.

Liu N.-K., Wang X.-F., Lu Q.-B. and Xu X.-M. (2009) Altered microRNA expression following traumatic spinal cord injury. *Exp. Neurol.* **219**, 424–429.

Liu C.-G., Wang J.-L., Li L., Xue L.-X., Zhang Y.-Q. and Wang P.-C. (2014) MicroRNA-135a and -200b, potential Biomarkers for Alzheimer's disease, regulate β secretase and amyloid precursor protein. *Brain Res.* **1583**, 55–64.

Liu L., Ye J.-X., Qin Y.-Z., Chen Q.-H. and Ge L.-Y. (2015) Evaluation of miR-29c, miR-124, miR-135a and miR-148a in predicting lymph node metastasis and tumor stage of gastric cancer. *Int. J. Clin. Exp. Med.* **8**, 22227–22236.

Liu Y., Liao S., Quan H., Lin Y., Li J. and Yang Q. (2016) Involvement of microRNA-135a-5p in the protective effects of hydrogen sulfide against Parkinson's disease. *Cell. Physiol. Biochem.* **40**, 18–26.

Liu N., Shi Y.-F., Diao H.-Y., Li Y.-X., Cui Y., Song X.-J., Tian X., Li T.-Y. and Liu B. (2017) MicroRNA-135a regulates apoptosis induced by hydrogen peroxide in rat cardiomyoblast cells. *Int. J. Biol. Sci.* **13**, 13–21.

Livak K. J. and Schmittgen T. D. (2001) Analysis of relative gene expression data using real-time quantitative PCR and the 2−ΔΔ $CT method. *Methods* **25**, 402–408.

Lorenz R., Bernhart S. H., HönerzuSiederdissen C., Tafer H., Flamm C., Stadler P. F. and Hofacker I. L. (2011) ViennaRNA Package 2.0. *Algorithms Mol. Biol.* **6**, 26.

Marcillo A., Frydel B., Bramlett H. M. and Dietrich W. D. (2012) A reassessment of P2X7 receptor inhibition as a neuroprotective strategy in rat models of contusion injury. *Exp. Neurol.* **233**, 687–692.

Mattes J., Yang M. and Foster P. S. (2007) Regulation of MicroRNA by Antagomirs. *Am. J. Respir. Cell Mol. Biol.* **36**, 8–12.

Meza-Sosa K. F., Valle-García D., Pedraza-Alva G. and Pérez-Martínez L. (2012) Role of microRNAs in central nervous system development and pathology. *J. Neurosci. Res.* **90**, 1–12.

Miras-Portugal M. T., Gomez-Villafuertes R., Gualix J., Diaz-Hernandez J. I., Artalejo A. R., Ortega F., Delicado E. G. and Perez-Sen R. (2016) Nucleotides in neuroregeneration and neuroprotection. *Neuropharmacology* **104**, 243–254.

Miska E. A., Alvarez-Saavedra E., Townsend M., Yoshii A., Sestan N., Rakic P., Constantine-Paton M. and Horvitz H. R. (2004) Microarray analysis of microRNA expression in the developing mammalian brain. *Genome Biol.* **5**, R68.

Mitchell C. H., Lu W., Hu H., Zhang X., Reigada D. and Zhang M. (2009) The P2X7 receptor in retinal ganglion cells: a neuronal model of pressure-induced damage and protection by a shifting purinergic balance. *Purinergic Signal.* **5**, 241–249.

Nakanishi K., Nakasa T., Tanaka N. *et al.* (2010) Responses of microRNAs 124a and 223 following spinal cord injury in mice. *Spinal Cord* **48**, 192–196.

Neary J. T., Rathbone M. P., Cattabeni F., Abbracchio M. P. and Burnstock G. (1996) Trophic actions of extracellular nucleotides and nucleosides on glial and neuronal cells. *Trends Neurosci.* **19**, 13–18.

Negulescu P. A. and Machen T. E. (1990) Intracellular ion activities and membrane transport in parietal cells measured with fluorescent dyes. *MethodsEnzymol.* **192**, 38–81.

Nieto-Diaz M., Esteban F. J., Reigada D., Muñoz-Galdeano T., Yunta M., Caballero-López M., Navarro-Ruiz R., Águila A. and Del Maza R. M. (2014) MicroRNAdysregulation in spinal cord injury: causes, consequences and therapeutics. *Front. Cell. Neurosci.* **8**, 53.

North R. A. and Jarvis M. F. (2013) P2X receptors as drug targets. *Mol. Pharmacol.* **83**, 759–769.

Orrenius S., Zhivotovsky B. and Nicotera P. (2003) Calcium: Regulation of cell death: the calcium–apoptosis link. *Nat. Rev. Mol. Cell Biol.* **4**, 552–565.

Ouzký M. (2002) Towards concerted efforts for treating and curing spinal cord injury. *Soc. Heal. Fam. Aff. Committee. Parliam. Assem. Counc. Eur.*, Doc 9401.

Peng W., Cotrina M. L., Han X., Yu H., Bekar L., Blum L., Takano T., Tian G.-F., Goldman S. A. and Nedergaard M. (2009) Systemic administration of an antagonist of the ATP-sensitive receptor P2X7 improves recovery after spinal cord injury. *Proc. Natl Acad. Sci. USA***106**, 12489–12493.

Peng B., Chen Y. and Leong K. W. (2015) MicroRNA delivery for regenerative medicine. *Adv. Drug Deliv. Rev.* **88**, 108–122.

Prentice H., Modi J. P. and Wu J.-Y. (2015) Mechanisms of neuronal protection against excitotoxicity, endoplasmic reticulum stress, and

mitochondrial dysfunction in stroke and neurodegenerative diseases. *Oxid. Med. Cell. Longev.* **2015**, 964518.

Reigada D., Navarro-Ruiz R. M., Caballero-López M. J., Águila Á., Del Muñoz-Galdeano T., Maza R. M. and Nieto-Díaz M. (2017) Diadenosine tetraphosphate (Ap4A) inhibits ATP-induced excitotoxicity: a neuroprotective strategy for traumatic spinal cord injury treatment. *Purinergic Signal.* **13**, 75–87.

Rodríguez-Zayas A. E., Torrado A. I. and Miranda J. D. (2010) P2Y2 receptor expression is altered in rats after spinal cord injury. *Int. J. Dev. Neurosci.* **28**, 413–421.

Rodríguez-Zayas A. E., Torrado A. I., Rosas O. R., Santiago J. M., Figueroa J. D. and Miranda J. D. (2011) Blockade of P2 nucleotide receptors after spinal cord injury reduced the gliotic response and spared tissue. *J. Mol. Neurosci.* **46**, 167–176.

Saugstad J. A. (2010) MicroRNAs as effectors of brain function with roles in ischemia and injury, neuroprotection, and neurodegeneration. *J. Cereb. Blood Flow Metab.* **30**, 1564–1576.

Sayed D. and Abdellatif M. (2011) MicroRNAs in development and disease. *Physiol. Rev.* **91**, 827–887.

Schneider C. A., Rasband W. S. and Eliceiri K. W. (2012) NIH Image to ImageJ: 25 years of image analysis.

Schwab J. M., Guo L. and Schluesener H. J. (2005) Spinal cord injury induces early and persistent lesional P2X4 receptor expression. *J. Neuroimmunol.* **163**, 185–189.

Selbach M., Schwanhäusser B., Thierfelder N., Fang Z., Khanin R. and Rajewsky N. (2008) Widespread changes in protein synthesis induced by microRNAs. *Nature* **455**, 58–63.

Strickland E. R., Hook M. A., Balaraman S., Huie J. R., Grau J. W. and Miranda R. C. (2011) MicroRNA dysregulation following spinal cord contusion: implications for neural plasticity and repair. *Neuroscience* **186**, 146–160.

Su Z., Yang Z., Xu Y., Chen Y. and Yu Q. (2015) MicroRNAs in apoptosis, autophagy and necroptosis. *Oncotargets. Oncotarget* **6**, 8474–8490.

Tremblay R. G., Sikorska M., Sandhu J. K., Lanthier P., Ribecco-Lutkiewicz M. and Bani-Yaghoub M. (2010) Differentiation of mouse Neuro 2A cells into dopamine neurons. *J. Neurosci. Methods* **186**, 60–67.

Volonté C., Parisi C. and Burnstock G. (2012) Purinergic signalling: what is missing and needed next? The use of transgenic mice, crystallographic analysis and MicroRNA. *CNS Neurol. Disord. Drug Targets* **11**, 751–767.

Wang X., Arcuino G., Takano T. *et al.* (2004) P2X7 receptor inhibition improves recovery after spinal cord injury. *Nat. Med.* **10**, 821–827.

Wang Y., Cui Y., Cui J., Sun L., Cui C., Zhang H., Zhu H., Li R., Tian Y. and Gao J. (2015) Neuroprotective effects of brilliant blue G on the brain following traumatic brain injury in rats. *Mol. Med. Rep.* **12**, 2149–2154.

Witkos T. M., Koscianska E. and Krzyzosiak W. J. (2011) Practical aspects of microRNA target prediction. *Curr. Mol. Med.* **11**, 93–109.

Yildiz-Unal A., Korulu S. and Karabay A. (2015) Neuroprotective strategies against calpain-mediated neurodegeneration. *Neuropsychiatr. Dis. Treat.* **11**, 297–310.

Yunta M., Nieto-Díaz M., Esteban F. J., Caballero-López M. J., Navarro-Ruíz R., Reigada D., Pita-Thomas D. W., Águila Á., Del Muñoz-Galdeano T. and Maza R. M. (2012a) MicroRNA dysregulation in the spinal cord following traumatic injury. *PLoS ONE* **7**, e34534.

Yunta M., Nieto-Díaz M., Esteban F. J., Caballero-López M., Navarro-Ruíz R., Reigada D., Pita-Thomas D. W., Águila A. del., Muñoz-Galdeano T. and Maza R. M. (2012b) MicroRNA dysregulation in the spinal cord following traumatic injury. *PLoS ONE* **7**, 000–000.

Zhang X., Zhang M., Laties A. M. and Mitchell C. H. (2005) Stimulation of P2X7 receptors elevates Ca2 + and kills retinal ganglion cells. *Invest. Ophthalmol. Vis. Sci.* **46**, 2183–2191.

Zhao J., Li X., Zou M., He J., Han Y., Wu D., Yang H. and Wu J. (2014) miR-135a inhibition protects A549 cells from LPS-induced apoptosis by targeting Bcl-2. *Biochem. Biophys. Res. Commun.* **452**, 951–957.

Zhao H., Zhang X., Dai Z., Feng Y., Li Q., Zhang J. H., Liu X., Chen Y. and Feng H. (2016) P2X7 receptor suppression preserves blood-brain barrier through inhibiting RhoA activation after experimental intracerebral hemorrhage in rats. *Sci. Rep.* **6**, 23286.

Zhou L., Luo L., Qi X., Li X. and Gorodeski G. I. (2009) Regulation of P2X7 gene transcription. *Purinergic Signal.* **5**, 409–426.

Zhu H.-J., Wang D.-G., Yan J. and Xu J. (2015) Up-regulation of microRNA-135a protects against myocardial ischemia/reperfusion injury by decreasing TXNIP expression in diabetic mice. *Am. J. Transl. Res.* **7**, 2661–2671.

Zuker M. (2003) Mfold web server for nucleic acid folding and hybridization prediction. *Nucleic Acids Res.* **31**, 3406–3415.